Journal of Nanophotonics

SPIEDigitalLibrary.org/jnp

From scattering regime to strong localization: a statistical analysis of the near-field intensity on random gold films

Julien Laverdant
Jean-Pierre Hermier
Xavier Quélin
Stéphanie Buil

SPIE

From scattering regime to strong localization: a statistical analysis of the near-field intensity on random gold films

Julien Laverdant,[a] Jean-Pierre Hermier,[b,c] Xavier Quélin,[b] and Stéphanie Buil[b]

[a]Université de Lyon, UMR5306 Université Lyon 1-CNRS, Institut Lumière Matière, 69622 Villeurbanne cedex, France

[b]Université de Versailles Saint-Quentin, Groupe d'Etudes de la Matière Condensée (UMR CNRS/UVSQ 8635), 45 avenue des Etats-Unis, 78035 Versailles, France
stephanie.buil@uvsq.fr

[c]Institut Universitaire de France, 103, boulevard Saint-Michel, F-75005 Paris, France

Abstract. Random metallic films have very specific optical properties due to disorder. Strong localization of electromagnetic fields can be observed due to plasmons. This localization strongly depends on excitation conditions, and different optical regimes can exist. To characterize these regimes, we investigated the spatial intensity correlation functions using near-field scanning optical microscopy for different excitation wavelengths and different incident polarization states. The transition between a weak scattering regime where no plasmon resonances are excited and a regime where strong plasmon resonances occur has clearly been observed. In the strong plasmonic regime, by varying the incident polarization direction, the shape of the correlation function has been correlated to the intensity enhancement which raises the possibility to control the intensity localization using the incident polarization state. [DOI: 10.1117/1.JNP.7.073589]

Keywords: near-field optics; random media; plasmonics.

Paper 12179SS received Dec. 14, 2012; revised manuscript received Jun. 26, 2013; accepted for publication Jun. 27, 2013; published online Aug. 8, 2013.

1 Introduction

Optical properties of metallic nanostructures have attracted great interest these last years.[1,2] For example, the energy localization that appears when surface plasmons are excited leads to a large number of applications in various fields, such as quantum information,[3] photovoltaic,[4] or optoelectronic devices.[5] Isolated metallic nanoparticules display localized plasmons with a narrow plasmon resonance frequency. More complex metallic nanostructures can support other light–metal interactions such as propagating plasmons or multiple-scattering of both evanescent and propagating waves.[6,7] When these nanostructures are coupled to light emitters[8,9] or photovoltaic components,[10] the kind of interaction is crucial for understanding and controlling the structure properties.

Among these complex nanostructures, the disordered metallic surfaces have been identified for strongly modifying emission properties of single emitters.[11,12] The disorder is responsible for the broad spectrum of plasmon resonances and for the strong localization of light.[13–15] To understand the transition between different regimes (plasmon resonances, scattering regime), we have studied the autocorrelation function (ACF) of near-field intensities for different incident light wavelengths and polarizations. In the pure scattering regime, we have already shown experimentally and theoretically that the ACF presents a very particular behavior. This behavior has been associated to the polarization-dependant coupling of evanescent waves and with the specific topography of the disordered nanostructure.[16,17] In this article, the evolution of the ACF from pure scattering to strong plasmon resonance regime is analyzed. In the case of strong plasmon resonance regime, the influence of the incident polarization is investigated.

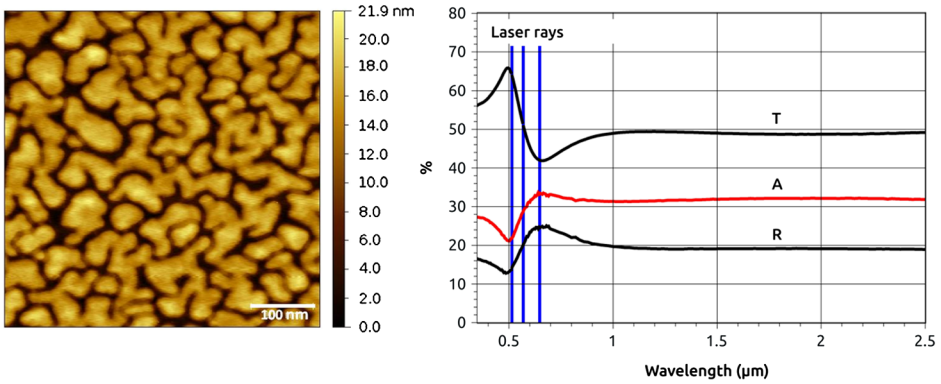

Fig. 1 (a) 500×500 nm^2 atomic force microscope (AFM) image of the disordered film. (b) Transmission (T), reflection (R) and absorption (A) spectra of the gold film near the percolation threshold. The laser lines at 514, 568, and 647 nm used in the experiments are also represented.

2 Samples Characterization

The disordered nanostructures under study are gold films elaborated by thermal evaporation. The gold concentration is adjusted just below the percolation threshold.[13] The morphology of the films is presented on the atomic force microscope image in Fig. 1(a). At the vicinity of this specific concentration, the film is semi-continuous and the gold clusters exhibit a wide range of sizes and shapes. Due to plasmon resonances on a broad range of frequencies, the absorption of the film is large (>30%). In Fig. 1(b), different regimes can be identified on the absorption curve. The absorption minimum is around 500 nm. It corresponds to a regime where no plasmons are excited on the film and corresponds to a pure scattering regime. For higher wavelengths, plasmon resonances are excited and the absorption increases. 530 nm is the plasmon resonance of an isolated gold cluster and higher wavelengths correspond to plasmon resonances of larger clusters. The absorption reaches a maximum value around 650 nm and from this value, the absorption looks like a "plateau." Between 500 and 650 nm, there is a transition between the pure scattering regime and the plasmonic regime.

In order to characterize this transition, experiments have been performed with an aperture scanning near-field optical microscope (SNOM), (Veeco, Bruker, Aurora 2, Madison). The sample is illuminated through a microscope objective by an Ar/Kr laser linearly polarized. The near-field intensity is collected through an Al-coated optical fiber. The incident polarization is controlled with a quarter wave plate and a polarizer. The sample-optical fiber distance is regulated by a shear forces feedback. The mapping of the near field intensity for different incident parameters (wavelength, polarization) on the same area of the sample can be performed. The set-up and typical SNOM images obtained with the apparatus have been described elsewhere.[13] 5×5 μm^2 optical images with 300×300 data points (resolution of 16 and 7 nm) are obtained and used for the analysis. Typical near-field optical images used for the ACF calculation can be seen in Ref. 13. The ACF of the intensities is defined as[16]

$$C(\Delta x, \Delta y) = \langle \delta I(x, y) \delta I(x + \Delta x, y + \Delta y) \rangle \tag{1}$$

with $\delta I(x, y) = [I(x, y) - \langle I(x, y) \rangle] / \langle I(x, y) \rangle$.

Each point of the ACF is calculated with the whole data points of the optical image. Each point corresponds to the same number of averages. The scale of the ACF is then smaller than the scale of the initial optical images. The distance between pixels is smaller than the half of the optical resolution. An accurate determination of the correlation radius is then possible. The ACF is not related to the particle size. The ACF of the topography can be seen in Ref. 16.

3 Transition from Pure Scattering Regime to Strong Plasmon Resonance Regime

To investigate the transition between a pure scattering regime and a strong plasmonic regime, three wavelengths are used, $\lambda = 514$ nm for the pure scattering regime, $\lambda = 647$ nm for the strong plasmonic regime, and $\lambda = 568$ nm for the transition regime. For these three wavelengths, the optical images used to calculate the intensity ACF have been obtained on the same area of the random surface and the linear polarization has been kept constant. These ACF are shown in Fig. 2, and the ACF along the x and y axis (corresponding to the polarization direction) are represented in Fig. 2(b), 2(d) and 2(f). All values are normalized by $C(0,0)$.

For the pure scattering regime ($\lambda = 514$ nm), the ACF has been experimentally and theoretically studied previously.[13] It always shows up an anisotropy in the direction of the incident polarization and oscillations perpendicular to this direction. The anisotropy has been attributed to a stronger coupling of evanescent waves in the direction of the incident polarization than in the orthogonal direction. The oscillations are due to the topography of the random film.

In the strong plasmonic regime ($\lambda = 647$ nm), the anisotropy of the ACF has nearly completely disappeared and the ACF becomes isotropic. In the intermediate regime ($\lambda = 568$ nm), the ACF is still anisotropic. The values of the anisotropic ratio κ defined in Ref. 15 are $\kappa = 1.38$ for $\lambda = 514$ nm, $\kappa = 1.35$ for $\lambda = 568$ nm and 0.96 for $\lambda = 647$ nm. This evolution is also a signature of the transition from the scattering to the plasmonic regime. The anisotropy can be due to near-field scattering that is dominant in the pure scattering regime. The plasmonic regime, at $\lambda = 647$ nm, is dominated by light localization leading to a more isotropic ACF (however, we will see in the next section that an anisotropy may appear in this regime, depending on the incident polarization). At $\lambda = 568$ nm, light scattering and light localization coexist.

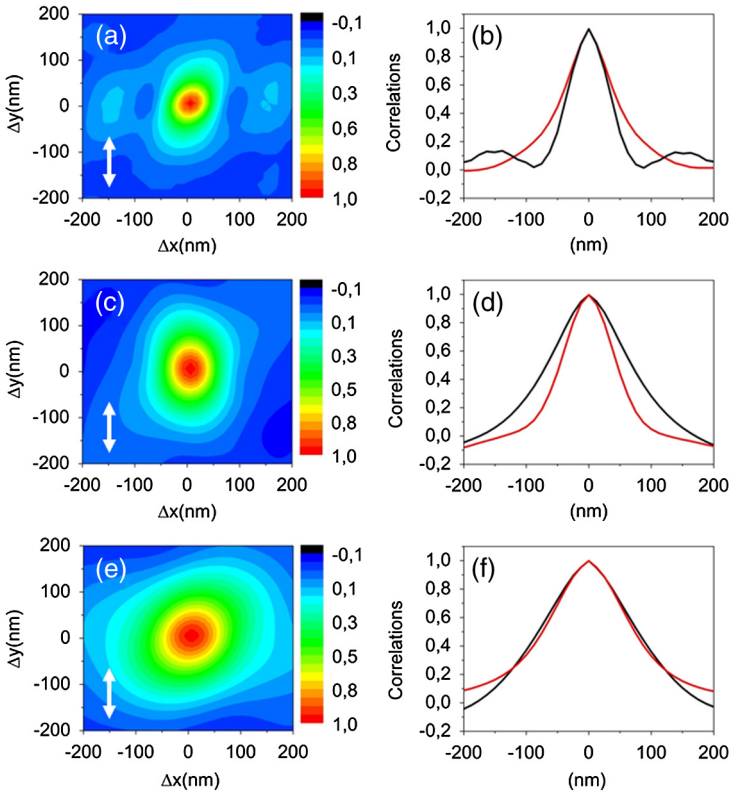

Fig. 2 ACF of near-field intensities for $\lambda = 514$ nm (a,b), $\lambda = 568$ nm (c,d) and $\lambda = 647$ nm (e,f). The 2D ACF are represented in the left column and the ACF in the x direction (red curve, perpendicular to the incident polarization direction) and the y direction (black curve, parallel to the incident polarization direction) are represented in the right column.

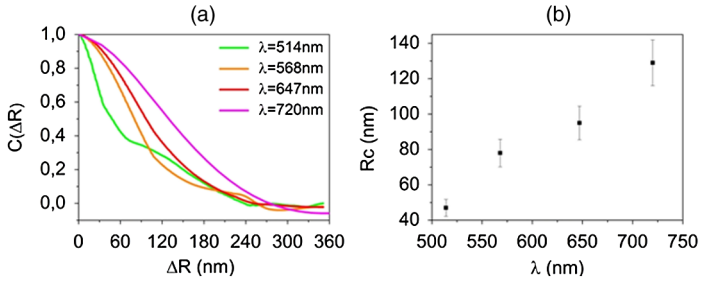

Fig. 3 (a) Normalized ACF $C(\Delta R)$ at constant distance for the four wavelengths that correspond to different regimes as described in the text. (b) Evolution of R_C with λ.

The ACF is larger than in the pure scattering regime and is still anisotropic. This can be explained by the coexistence of both regimes at this wavelength.

Moreover, the mean radius of the ACF in any direction increases with the wavelength. To investigate this point, an average correlation function is defined. This function is

$$C(\Delta R) = \langle C(\Delta x, \Delta y) \rangle_{\Delta R = \sqrt{\Delta x^2 + \Delta y^2}}, \tag{2}$$

where an average of the ACF is made at a distance ΔR. The results obtained for the different wavelengths are presented in Fig. 3. The correlation function is normalized by $C(0)$. In this figure, a fourth wavelength ($\lambda = 720$ nm) has been added. This experiment was not performed on the same area than the other wavelengths because another laser had to be used. However, this wavelength illustrates the general tendency for the mean radius to increase with the wavelength.

The function $C(\Delta R)$ is larger as the wavelength is higher. A mean correlation radius R_C can be defined as the radius of the half width at full maximum. The values of this radius are $R_C =$ 47 nm for $\lambda = 514$ nm, 78 nm for $\lambda = 568$ nm, 95 nm for $\lambda = 647$ nm, and 129 nm for $\lambda = 720$ nm.

It has been shown that in the plasmonic regime, the energy is localized in hot spots situated in between clusters.[13] As the wavelength increases, the energy is more and more localized. The number of hot spots decreases but their energy is higher. The localization of light is stronger when the wavelength increases. This induces a change in the shape of the ACF that becomes wider for higher wavelengths. These results show that the shape and the width of the ACF exhibit characteristics of the different regimes of light-gold surface interactions.

4 Polarization Dependence in the Plasmon Regime

In this section, the influence of the incident polarization is studied. A strong dependence on the incident polarization has already been observed in the scattering regime.[16] In this case, the ACF is always anisotropic with the longest axis parallel to the polarization direction. In the plasmonic regime, the energy is localized and the dependence of the hot spots position on the incident polarization has been pointed out in different studies. It has been theoretically[18] predicted and experimentally observed[19,20] that the position of some hot spots changes when the incident polarization is modified. However some of them seem to remain at the same position. This question is of fundamental interest as the polarization could be a good way to address some specific areas of energy.

The ACF has been studied in the strong plasmon regime, at $\lambda = 647$ nm, for different incident polarizations. In the same way as in Sec. 3, SNOM images have been obtained on the same area with different incident polarizations. ACF has been deduced from these SNOM images. Eight linear polarizations have been used (5×5 μm^2 optical images with a resolution of 25 nm), ACF for 0, 45, and 90 deg are presented in Fig. 4.

In Fig. 4, several behaviors are clearly visible. The ACF can be isotropic or not, depending on the incident polarization. The anisotropic case (45 deg) appears to be related to the incident polarization.

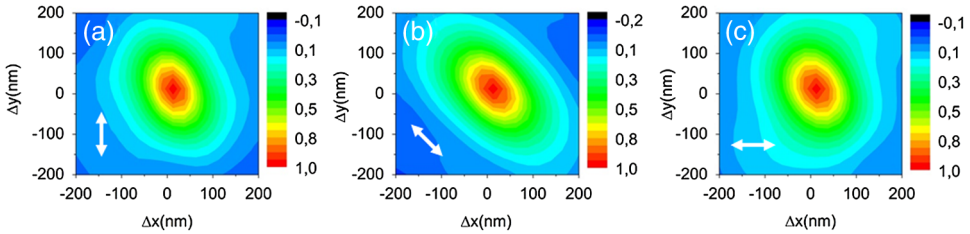

Fig. 4 ACF for three polarizations, 0 deg (a), 45 deg (b) and 90 deg (c) at $\lambda = 647$ nm.

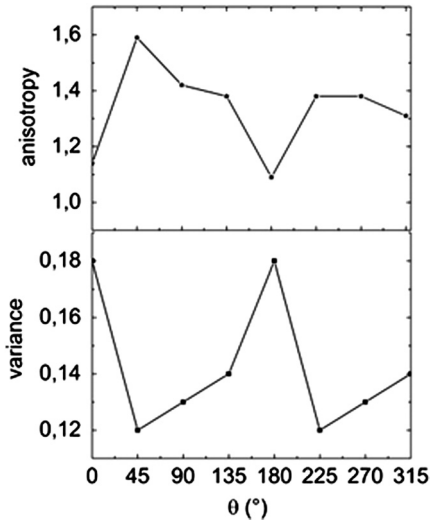

Fig. 5 Anisotropy (a) and variance (b) for eight polarizations at $\lambda = 647$ nm.

For a better understanding of this anisotropy, the spatial variance of the intensity distribution has been calculated for each polarization. This function is related to the local field enhancements. In Fig. 5, the anisotropy factor and the variance for the eight polarizations are plotted.

An anti-correlation between the variance and the anisotropy is observed. The variance is maximum when the anisotropy is minimum and the variance is minimum when the anisotropy is maximum. The behavior of these two parameters is clearly linked. The variance is maximum when the field enhancement is maximum, which means that the localization of light is maximum. In this case, the ACF becomes isotropic because the localization of the energy is stronger. When the variance decreases, the ACF becomes anisotropic. In these cases, the energy is less localized and scattering or delocalized plasmon modes may be at the origin of the anisotropy of the ACF.[21,22]

A direct relationship between the correlation maps and the direction of the incident field polarization is not obvious. In an assembly of nanoparticles, the field enhancement depends on the orientation of the polarization versus the junction between particles.[23,24] It is possible to link the field enhancement to the incident polarization. The situation is more complex for random films where hot spots are randomly generated on the film. From an experimental point of view, hot spots are due to the local environment that can be isotropic or not. Therefore, the angle of the field polarization cannot be related to the local metallic shapes. It is difficult to predict how different areas of the film will be affected by the polarization. A last way to illustrate the influence of the incident polarization consists in the autocorrelation of SNOM images obtained for the different incident polarizations. The correlation between points of two images with a polarization angle difference $\Delta\theta$ is performed. Therefore, the polarization correlation $C(\Delta\theta)$ is defined as

$$C(\Delta\theta) = \langle I(r,\theta)I(r,\theta+\Delta\theta)\rangle / [\langle I(r,\theta)\rangle\langle I(r,\theta+\Delta\theta)\rangle]. \quad (3)$$

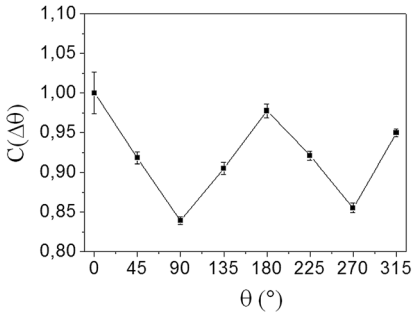

Fig. 6 Polarization correlation function $C(\Delta\theta)$.

The average is made over the whole points of the images and over all the images with a polarization difference $\Delta\theta$. For example C (45 deg) is the average of the correlation between images at 0 and 45 deg, 45 and 90 deg, 90 and 135 deg, 135 and 180 deg, 180 and 225 deg, 225 and 270 deg, 270 and 315 deg, and 315 and 360 deg. The results are presented in Fig. 6.

As expected, a periodicity of 180 deg for the correlation in polarization is observed with maxima for 0 and 180 deg and minima for 90 and 270 deg. The maximum deviations are obtained for optical maps with crossed polarization ($\Delta\theta = 90$ deg). The relative variation between the maximum and the minimum is a quantitative tool to point out the differences between optical images obtained for different polarizations. The contrast between the maximum and the minimum is around 15%. This value indicates that qualitatively 15% of the images change with the polarization.

5 Conclusion

Random metallic films are complex structures that can support many different regimes of light matter interactions. The statistical analysis of near-field intensities in terms of intensity correlation functions can highlight various behaviors. On the other hand, regimes where light scattering is dominant are characterized by anisotropic and smaller ACF. In regimes where plasmons are excited, wider and more isotropic ACF are observed. This is due to the localization of the energy on small areas. A dependence on the incident polarization is observed on the ACF. This can hardly be linked to the structure. The use of a polarization correlation function $C(\Delta\theta)$ is a way to address a part of this problem. In the case of random structures, it shows that 15% of the near-field intensity depends on the incident polarization in the visible range.

Acknowledgments

The near-field experiments presented in this manuscript were performed by Julien Laverdant and Stéphanie Buil. Statistical analysis was performed by Julien Laverdant who was a PhD student at the time of these experiments. His work was supervised by Stéphanie Buil and Xavier Quélin. Jean-Pierre Hermier is at the head of the team and participated to the writing and analysis of this manuscript.

References

1. V. A. Markel and T. F. Georges, Eds., *Optics of Nanostructured Materials*, Wiley Interscience, New York (2001).
2. V. Giannini et al., "Plasmonic nanoantennas: fundamentals and their use in controlling the radiative properties of nanoemitters," *Chem. Rev.* **111**(6), 3888 (2011), http://pubs.acs.org/doi/abs/10.1021/cr1002672.
3. R. Esteban, T. V. Teperik, and J. J. Greffet, "Optical patch antennas for single photon emission using surface plasmons," *Phys. Rev. Lett.* **104**(2), 026802 (2010), http://dx.doi.org/10.1103/PhysRevLett.104.026802.

4. I. M. Pryce et al., "Plasmonic nanoparticle enhanced photocurrent in GaN/InGaN/GaN quantum well solar cells," *App. Phys. Lett.* **96**(15), 153501 (2010), http://dx.doi.org/10.1063/1.3377900.
5. E. K. Keshmarzi, Z. N. Tait, and P. Berini, "Long-range surface plasmon single-mode laser concepts," *J. Appl. Phys.* **112**(6), 063115 (2012), http://dx.doi.org/10.1063/1.4754417.
6. N. Salerno et al., "Near-field optical response of a two-dimensional grating of gold nanoparticles," *Phys. Rev. B* **63**(16), 165422 (2001), http://dx.doi.org/10.1103/PhysRevB.63.165422.
7. A. Apostal and A. Dogariu, "Non-Gaussian statistics of optical near-fields," *Phys. Rev. E* **72**(2), 025602 (2005), http://dx.doi.org/10.1103/PhysRevE.72.025602.
8. J. Barthes et al., "Purcell factor for a point-like dipolar emitter coupled to a two-dimensional plasmonic waveguide," *Phys. Rev. B* **84**(7), 073403 (2011), http://dx.doi.org/10.1103/PhysRevB.84.073403.
9. D. E. Chang et al., "Strong coupling of single emitters to surface plasmons," *Phys. Rev. B* **76**(3), 035420 (2007), http://dx.doi.org/10.1103/PhysRevB.76.035420.
10. Y. Harada et al., "Plasmon-induced photocurrent changes in GaAs photovoltaic cells modified with gold nanospheres: a near-field imaging study," *J. Appl. Phys.* **110**(10), 104306 (2011), http://dx.doi.org/10.1063/1.3662114.
11. I. Mallek-Zouari et al., "Plasmon assisted single photon emission of CdSe/CdS nanocrystals deposited on random gold film," *Appl. Phys. Lett.* **97**(5), 053109 (2010), http://dx.doi.org/10.1063/1.3467264.
12. R. Sapienza et al., "Long-tail statistics of the Purcell factor in disordered media driven by near-field interactions," *Phys. Rev. Lett.* **106**(16), 163902 (2011), http://dx.doi.org/10.1103/PhysRevLett.106.163902.
13. S. Buil et al., "Local field intensity enhancements on gold semicontinuous films investigated with an aperture nearfield optical microscope in collection mode," *J. Appl. Phys.* **100**(6), 063530 (2006), http://dx.doi.org/10.1063/1.2335664.
14. S. Grésillon et al., "Experimental observation of localized optical excitations in random metal-dielectric films," *Phys. Rev. Lett.* **82**(22), 4520 (1999), http://dx.doi.org/10.1103/PhysRevLett.82.4520.
15. Y. Nishijima, L. Rosa, and S. Juodkazis, "Surface plasmon resonances in periodic and random patterns of gold nano-disks for broadband light harvesting," *Opt. Express* **20**(10), 11455 (2012), http://dx.doi.org/10.1364/OE.20.011466.
16. J. Laverdant et al., "Polarization dependent near-field speckle of random gold films," *Phys. Rev. B* **77**(16), 165406 (2008), http://dx.doi.org/10.1103/PhysRevB.77.165406.
17. J. Laverdant et al., "Near-field intensity correlations on nanosclaed random silver/dielectric films," *J. Nanophoton.* **4**(1), 049505 (2010), http://dx.doi.org/10.1117/1.3506519.
18. S. Buil et al., "FDTD simulations of localization and enhancements on fractal plasmonics nanostructures," *Opt. Express* **20**(11), 11968 (2012), http://dx.doi.org/10.1364/OE.20.011968.
19. S. Ducourtieux et al., "Near-field optical studies of semicontinuous metal films," *Phys. Rev. B.* **64**(16), 165403 (2001), http://dx.doi.org/10.1103/PhysRevB.64.165403.
20. R. C. Word, J. Fitzgerald, and R. Könenkamp, "Photoelectron emission control with polarized light in plasmonic metal random structures," *App. Phys. Lett.* **99**(4), 041106 (2011), http://dx.doi.org/10.1063/1.3615783.
21. M. I. Stockman, S. V. Faleev, and D. Bergman, "Localization versus delocalization of surface plasmons in nanosystems: can one state have both characteristics?," *Phys. Rev. Lett.* **87**(16), 167401 (2001), http://dx.doi.org/10.1103/PhysRevLett.87.167401.
22. K. Seal et al., "Coexistence of localized and delocalized surface plasmon modes in percolating metal films," *Phys. Rev. Lett.* **97**(20), 206103 (2006), http://dx.doi.org/10.1103/PhysRevLett.97.206103.
23. H. Wei et al., "Polarization dependence of surface-enhanced Raman scattering in gold nanoparticle–nanowire systems," *Nano. Lett.* **8**(8), 2497–2502 (2008), http://dx.doi.org/10.1021/nl8015297.
24. H. Xu and M. Käll, "Polarization-dependent surface-enhanced Raman spectroscopy of isolated silver nanoaggregates," *ChemPhysChem* **4**(9), 1001 (2003), http://dx.doi.org/10.1002/cphc.v4:9.

Julien Laverdant has received his PhD in optics and photonics in 2007 at the University of Versailles Saint Quentin on the optical properties of random gold films. Then, he focused on the control of single photon sources using optical modes in photonic and plasmonic crystals. He became an associate professor in 2011. At present, he studies the optical properties of plasmon–emitter interactions in the weak and strong coupling regimes for nanophotonic applications.

Jean-Pierre Hermier received a PhD in quantum physics in 2000 at the Université Pierre & Marie Curie and an "Habilitation à Diriger des Recherches" in 2005. He is currently a professor at the Université Versailles St-Quentin. His current research interests are quantum optics, plasmonics and semiconductor nanocrystals.

Xavier Quelin received a PhD in condensed matter physics in 1993 at the Université Pierre & Marie Curie and an "Habilitation à Diriger des Recherches" in 2011. He is currently an assistant professor at the Université Versailles St-Quentin. His current research interests are, from experimental or numerical points of view, plasmonics in random media and localization effects. He is also involved in the field of nanophotonics like optical properties of semiconductor nanocrystals.

Stéphanie Buil received a PhD in physics in 1998 at the University Bordeaux I and an "Habilitation à Diriger des Recherches" in 2010. Since 1999, she has been an assistant professor at the University of Versailles. She is interested in near-field plasmonic and in interaction between single fluorescent emitters and plasmonic structures.